

# Symmetric Superconducting Dome Accompanied by Non-Fermi Liquid Transport in Ionic Liquid Gated-MoS<sub>2</sub>

Qiao Chen<sup>1</sup>, Changshuai Lan<sup>1</sup>, Huiqin Jian<sup>1</sup>, Yi Yan<sup>1</sup>, Xinming Zhao<sup>1</sup>, Yihang Li<sup>1</sup>,  
Huai Guan<sup>1</sup>, Nina Girotto Erhardt<sup>2</sup>, Dino Novko<sup>2</sup>, Bo Gao<sup>3</sup>, Chengyu Yan<sup>\*,1,4</sup>, Shun  
Wang<sup>\*,1,4</sup>

<sup>1</sup>MOE Key Laboratory of Fundamental Physical Quantities Measurement & Hubei Key  
Laboratory of Gravitation and Quantum Physics, National Gravimetry Laboratory and  
School of Physics, Huazhong University of Science and Technology, Wuhan 430074,  
China

<sup>2</sup>Centre for Advanced Laser Techniques, Institute of Physics, Zagreb 10000, Croatia.

<sup>3</sup>Tsung-Dao Lee Institute, Shanghai Jiao Tong University, Shanghai 201210, People's  
Republic of China

<sup>4</sup>Institute for Quantum Science and Engineering, Huazhong University of Science and  
Technology, Wuhan 430074, China

Corresponding Authors: Chengyu Yan (chengyu\_yan@hust.edu.cn); Shun Wang  
(shun@hust.edu.cn)

## Abstract

In strongly correlated superconductors, the emergence of superconductivity is often accompanied by anomalous normal state. The connection between these two phenomena is considered crucial for understanding the underlying unconventional pairing mechanisms. In this study, we report analogous behavior in MoS<sub>2</sub>, a band insulator devoid of long-range magnetic order. Through ionic liquid gating, continuous doping control from the underdoped to the overdoped regime was achieved, revealing

a symmetric superconducting dome that holds characteristic scaling relations mirror the behavior of strongly correlated superconductors. Strikingly, this system exhibits pronounced non-Fermi liquid transport near optimal doping, characterized by a quasi-linear temperature dependence of resistivity over a wide range and a  $T^2$ -dependent Hall angle cotangent. The strength of the non-Fermi liquid transport is positively correlated with the superconducting transition temperature, with both evolving synchronously across the phase diagram. These results highlight the potential of MoS<sub>2</sub> as an ideal platform for studying the intrinsic connection between non-Fermi liquid transport and superconductivity.

## Introduction

In the study of strongly correlated superconductors, the intimate connection between superconductivity and normal-state transport holds a key to understand their unconventional pairing mechanisms<sup>[1-15]</sup>. In such systems like cuprates<sup>[1-4]</sup> and iron-based superconductors<sup>[5-7, 14]</sup>, the emergence of the superconducting dome is invariably accompanied by normal state transport properties that starkly violate the Fermi liquid picture. This recurrent conjunction suggests that both phenomena are underpinned by common physical origin. However, the complex interplay of competing orders and multiple degrees of freedom in these materials obscures the intrinsic physical link between these two phenomena.

Transition metal dichalcogenides (TMDs) offer the possibility to study this problem in a simpler context. These materials not only exhibit properties similar to strongly correlated superconductors, such as two-dimensional superconductivity<sup>[16-18]</sup>, coexistence of charge density waves<sup>[19-21]</sup>, and characteristic dome-shaped superconducting phase diagrams<sup>[22-25]</sup>, but also hold the clear observations of non-Fermi liquid transport<sup>[26]</sup>.

Nonetheless, relevant studies in TMDs systems still face significant challenges. For the study of superconductivity, the origin of the superconducting dome and its underlying mechanism are still central open questions. Diverse theoretical scenarios have been proposed for TMDs, including enhanced electron-phonon coupling from

multi-valley scattering<sup>[23, 27]</sup>, correlation-driven renormalization of quasiparticles<sup>[28]</sup>, structural instability and soft phonon modes associated with charge density waves<sup>[29]</sup>. This lack of consensus highlights the pressing need for experimental evidence to explore the superconducting mechanism. For the study of non-Fermi liquid transport, it has been reported in 2M-WS<sub>2</sub><sup>[26]</sup>, where constraints of the doping method have limited further systematic exploration. Notably, in twisted-TMDs and other moiré systems, both the superconducting dome and non-Fermi liquid transport also emerge concomitantly<sup>[11, 30]</sup>. However, their behaviors are extremely sensitive to the moiré twist angle, and consequently, fluctuations of the rotation angle during fabrication introduce uncertainty in studying their intrinsic physical properties.

Against this backdrop, electrostatic doping-induced superconductivity in TMDs demonstrates unique value. Taking MoS<sub>2</sub> as an example, the ionic liquid gating method can inject carriers into MoS<sub>2</sub> via electrostatic doping, enabling continuous tuning from an insulating to a metallic and finally a superconducting state<sup>[22, 23, 31]</sup>. The ground state of MoS<sub>2</sub> is a band insulator, and no long-range magnetic order has been observed in its phase diagram<sup>[22]</sup>, providing an ideal platform for studying superconductivity and normal state behavior. However, although the underdoped regime of MoS<sub>2</sub> is well-established by several works<sup>[22, 23]</sup>, the further effort to map the complete superconducting dome has received less attention, thereby hindering a conclusive discussion on the underlying superconducting mechanism. Simultaneously, systematic investigation of its normal state is still relatively lacking. These two gaps prevent the establishment of a clear link between superconductivity and normal state transport in MoS<sub>2</sub>.

Addressing these issues, this study achieves continuous tuning of MoS<sub>2</sub> from the underdoped to the overdoped regime by precisely calibrating the dependence of carrier concentration on gate voltage, and observes a symmetric superconducting dome. Further transport measurements reveal that the normal state near optimal doping exhibits significant non-Fermi liquid transport behaviour, whose strength evolves synchronously with the superconducting transition temperature ( $T_c$ ) across the whole phase diagram. These results provide key evidence for understanding the

superconductivity in MoS<sub>2</sub> and highlight the potential of this system as an ideal platform for studying superconductivity and non-Fermi liquid transport.

## Result and discussion

This study employs dual-gated ionic liquid-MoS<sub>2</sub> devices with a standard Hall bar structure (inset of Figure 1b, see “Methods” for details) for electrical transport measurements. When an ionic gate voltage ( $V_{ig}$ ) is applied to ionic liquid DEME-TFSI (N,N-diethyl-N-methyl-N-(2-methoxyethyl) ammonium bis (trifluoromethylsulfonyl)-imide), ions accumulate and inject carriers at the ionic liquid-MoS<sub>2</sub> interface, driving an insulator-metal transition and ultimately inducing superconductivity<sup>[16, 17, 22]</sup>. A key prerequisite for systematically studying the superconducting phase diagram of MoS<sub>2</sub> is to accurately establish the correspondence between carrier concentration ( $n_{2D}$ ) and  $V_{ig}$ . Contrary to expectations based on a basic capacitor model, a large  $V_{ig}$  causes the ion arrangement to become dense and form “trapped bands” (Figure 1a), leading to the localization of some carriers in Coulomb potential traps, which in turn causes  $n_{2D}$  and conductivity to exhibit a non-monotonic dependence on  $V_{ig}$  (Figure 1b)<sup>[32, 33]</sup>. A direct calibration of  $n_{2D}$  via Hall measurements at 15 K shows that the maximal  $n_{2D}$  of the device reaches  $17 \times 10^{13} \text{ cm}^{-2}$ , significantly exceeding the range of the underdoped region (below  $12 \times 10^{13} \text{ cm}^{-2}$ )<sup>[22, 23]</sup>, indicating the potential to explore the overdoped region.

Fig. 1c shows the  $R$ - $T$  curves at a fixed  $V_{ig}$  for a typical device. This device exhibits a sharp superconducting transition around 10 K, with resistance dropping to zero. Its superconducting characteristics are highly consistent with previous reports<sup>[16, 17, 34]</sup>, in which the superconducting transition is strongly suppressed by an out-of-plane magnetic field (Figure 1d), while it remains relatively stable under an in-plane magnetic field (see “Supplementary Information Section 3” for more details), displaying typical Ising superconductivity characteristics. These results are consistent with existing research on high-quality ionic liquid-induced superconducting MoS<sub>2</sub>, confirming the reliability of the device performance in this study and laying the experimental foundation for subsequent systematic research.

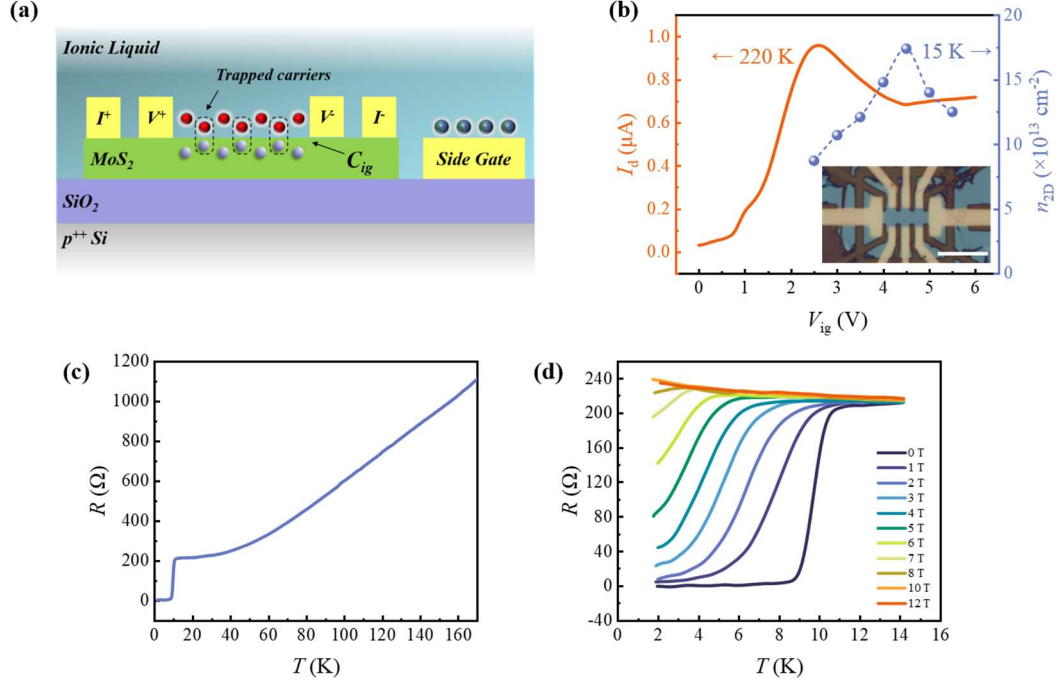


**Figure 1.** Transport properties of ionic liquid-gated MoS<sub>2</sub> devices. **(a)** Schematic of the device structure. Cations form a zigzag packing at the MoS<sub>2</sub> interface and induce a 2D electron gas. Excessively close ions create Coulomb potential traps that can localize electrons. The green bar represents the MoS<sub>2</sub> crystal etched into a standard Hall bar structure. Gold squares represent Ti/Au electrodes, grey spheres representing cations. The blue transparent one is ionic liquid DEME-TFSl, with blue spheres representing anions and red spheres representing cations. The purple and grey layers represent the 285 nm SiO<sub>2</sub> and p<sup>++</sup> Si substrate, respectively. **(b)** Transfer characteristic curve (left axis) and the  $n_{2D}$ - $V_{ig}$  curve (right axis). Inset: Optical micrograph of a typical device. Scale bar: 10  $\mu$ m. **(c)**  $R$ - $T$  curve for a typical superconducting MoS<sub>2</sub> device, showing a sharp superconducting transition. **(d)**  $R$ - $T$  curve under out-of-plane magnetic field for the device in (c).

Based on the established  $n_{2D}$ - $V_{ig}$  relationship and measurement protocol, we systematically measured the low-temperature transport properties of the device within the  $V_{ig}$  range of 2 to 4.5 V. In this range,  $n_{2D}$  increases monotonically with  $V_{ig}$ , facilitating controlled parameter scanning, while the region with  $V_{ig} > 4.5$  V is not included in this analysis due to excessively strong trapped bands effect. Figure 2a shows the  $R$ - $T$  curves at different  $n_{2D}$  values. The superconducting critical temperature  $T_c$  shows a non-monotonic variation with  $n_{2D}$ , reaching a peak of about 10 K at  $n_{2D} = 12.1 \times 10^{13} \text{ cm}^{-2}$ , consistent with the reported optimal doping point in MoS<sub>2</sub><sup>[22, 23]</sup>. As  $n_{2D}$  increases further,  $T_c$  gradually decreases, indicating the system enters the overdoped region. Meanwhile, the normal state resistance decreases monotonically with increasing  $n_{2D}$ , without showing the insulating re-entrant behavior observed in WS<sub>2</sub><sup>[24, 33]</sup>, ruling

out the possibility that a decrease in  $n_{2D}$  causes the reduction in  $T_c$ . Control experiments with a back gate confirmed the assigned doping regimes are discussed in Supplementary Sections 4. The resulting superconducting phase diagram is shown in Figure 2b, exhibiting a symmetric dome structure centered around the optimal doping point. This morphology is similar to phase diagrams reported for other TMDs superconductors like  $\text{TiSe}_2$ <sup>[19]</sup>,  $\text{TaS}_2$ <sup>[35]</sup>, and twisted  $\text{WSe}_2$ <sup>[11, 36, 37]</sup>, suggesting that symmetric superconducting domes might be a universal characteristic of TMDs superconductors.

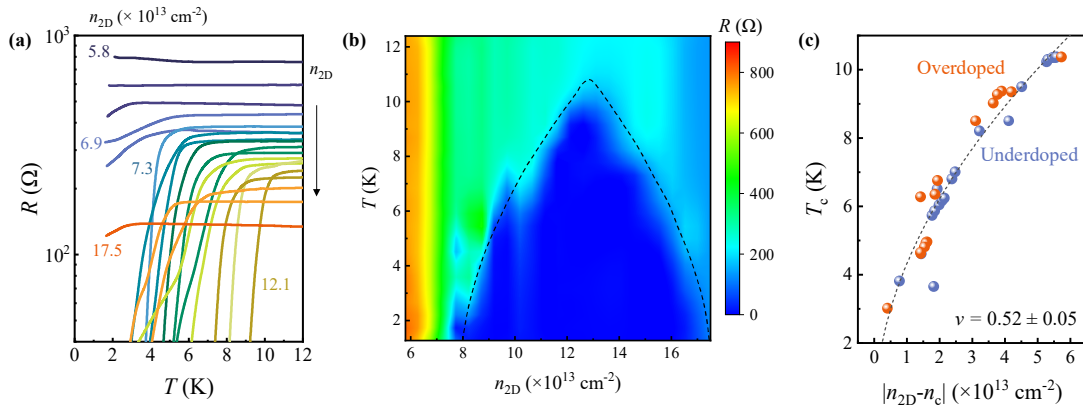


**Figure 2.** The superconducting dome in ionic-MoS<sub>2</sub> devices. **(a)**  $R$ - $T$  curves measured at different  $n_{2D}$ , showing the evolution of the superconducting transition, showing a non-monotonic variation of the superconducting transition with  $n_{2D}$ . **(b)** Superconducting phase diagram constructed from the data in (a), plotting the superconducting transition temperature  $T_c$  as a function of  $n_{2D}$ . The symmetric dome centers at the optimal doping level of  $n_{2D} \sim 12.1 \times 10^{13} \text{ cm}^{-2}$  with a maximum  $T_c \sim 10 \text{ K}$ . **(c)** Normalized superconducting phase diagram with overlapping underdoped and overdoped regions, the dashed line fitted by  $T_c \propto |n - n_c|^\nu$ .

The shape of a superconducting dome provides crucial insight into the underlying pairing mechanism. To date, the origin of the superconducting dome in MoS<sub>2</sub> remains an open question, with proposed mechanisms focusing on several competing scenarios: enhanced electron-phonon coupling due to multivalley Fermi surface evolution<sup>[23]</sup>, competition between intervalley phonon scattering strength and screening<sup>[27]</sup>, phonon softening associated with structural instabilities such as charge density waves<sup>[29]</sup>, and quasiparticle renormalization governed by electron correlation effects<sup>[28]</sup>. These mechanisms typically rely on the competition between two opposing trends during doping to explain the non-monotonic variation of the superconducting  $T_c$ . However, such models dominated by two distinct physical processes often struggle

to produce the highly symmetric dome shape observed experimentally.

In contrast, symmetric superconducting domes are frequently observed in strongly correlated superconductors, such as cuprates, iron-based superconductors, heavy-fermion systems, and twisted-2D materials. In these systems, the critical temperature often follows a universal scaling relation with doping concentration<sup>[5]</sup>,  $T_c \propto |n-n_c|^\nu$ , where  $n$  is the doping level,  $n_c$  is the critical doping at the dome boundary, and  $\nu$  is the critical exponent, reflecting the divergence of the order parameter's coherence length upon approaching  $n_c$ . The value of  $\nu$  serves to identify the universality class of the phase transition, typically falling within the range of  $0.5 \sim 0.6$  for the aforementioned strongly correlated superconductors<sup>[5]</sup>.

The extracted critical exponents of MoS<sub>2</sub> in our study are  $\nu = 0.52 \pm 0.05$  with  $n_c = 6.57 \times 10^{13} \text{ cm}^{-2}$  on the underdoped side, and  $n_c = 17.91 \times 10^{13} \text{ cm}^{-2}$  on the overdoped side. This  $\nu$  value agree well with those reported for various cuprate and iron-based superconductors<sup>[5, 38-40]</sup>. Notably, the both side of superconducting dome of MoS<sub>2</sub> are almost identical (Figure 2c), indicating a symmetric suppression of the superconducting order parameter. This symmetry suggests that the entire superconducting dome may be governed by a unified quantum critical point, further supporting the similarity between MoS<sub>2</sub> and strongly correlated superconductors.

To further examine the similarity between MoS<sub>2</sub> and other strongly correlated superconductors, we calculated the ratio of the superconducting transition temperature to the Fermi temperature ( $T_c/T_F$ ). The Fermi temperature  $T_F$  for MoS<sub>2</sub> is estimated from  $n_{2D}$  using the free electron gas model.  $T_c/T_F$  is a key indicator for distinguishing conventional BCS superconductivity from strongly correlated superconductivity.  $T_c/T_F \ll 0.01$  belongs to weak-coupling BCS superconductor (e.g., conventional metals like aluminum, grey squares in Figure 3), where electron pairing is primarily mediated by electron-phonon interactions. Higher  $T_c/T_F$  values signify strongly correlated superconductivity (e.g., cuprate, iron-based, and heavy-fermion superconductors, blue shaded region in Figure 3), often involving non-BCS mechanisms such as electron-electron interactions. The  $T_c/T_F$  value for optimal doped MoS<sub>2</sub> in this study lies precisely at the boundary of this critical region (Orange diamonds in Figure 4), indicating that its superconducting mechanism significantly deviates from the

traditional BCS picture and is closer to the realm of strongly correlated superconductivity.

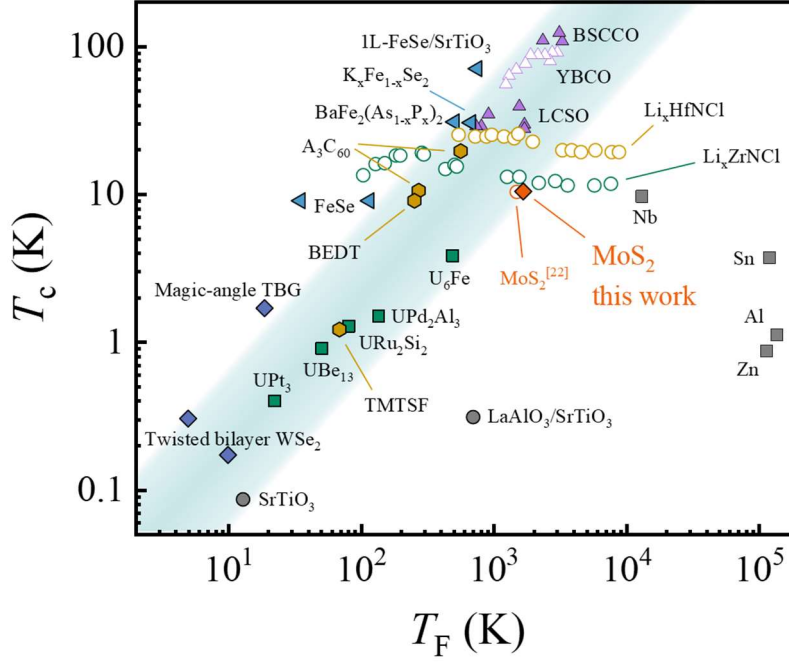


Figure 3. Comparison of superconductors on the  $T_c/T_F$  scale. The superconducting transition temperature  $T_c$ , normalized by the Fermi temperature  $T_F$ , serves as a key metric for correlation strength. The blue shaded region marks the range occupied by most strongly correlated superconductors (e.g., cuprates, iron-based, heavy-fermion)<sup>[11, 22, 34, 37, 41-49]</sup>. The position of optimal doped MoS<sub>2</sub> from this work (orange diamonds) and report<sup>[22]</sup> (orange open circle) at the boundary of this region indicates its departure from the conventional BCS regime and places it within the realm of correlated superconductors.

Having given the observed similarities between MoS<sub>2</sub> and strongly correlated superconductors discussed above, a critical question naturally arises: does the normal state accompanying superconductivity in MoS<sub>2</sub> also exhibit corresponding anomalous behavior? In strongly correlated superconductors such as cuprates, iron-based, and heavy-fermion systems, there often exists a profound physical connection between the superconducting state and its normal state. Understanding the properties of this normal state is essential for uncovering the underlying superconducting mechanism.

As shown in Figure 4a, the temperature-dependent resistance ( $R$ - $T$ ) relationship of an optimal doped device ( $n_{2D} = 12.5 \times 10^{13} \text{ cm}^{-2}$ ,  $T_c = 9.8 \text{ K}$ ) reveals clear deviations from Fermi-liquid behavior. A scaling analysis using  $R = R_0 + A \times T^\alpha$  yields  $\alpha = 1.19$  over the temperature range 60 ~ 170 K, significantly departing from the Fermi-liquid

expectation of  $\alpha = 2$ . This provides clear evidence of non-Fermi liquid transport in the system, further strengthening the analogy to established correlated superconductors. Simultaneously, multiple devices near optimal doping exhibit non-Fermi liquid transport characteristics with  $\alpha \rightarrow 1$  (see ‘‘Supplementary Section 6’’ for more details), confirming the intrinsic and reproducible nature of this phenomenon.

To further confirmed the existence of non-Fermi liquid transport behavior in optimally doped MoS<sub>2</sub>, we measured the Hall angle, defined as  $\Theta_H = \arctan(\sigma_{xy}/\sigma_{xx})$  where  $\sigma_{xy}$  and  $\sigma_{xx}$  are the Hall and longitudinal conductivities respectively. The cotangent of Hall angle,  $\cot(\Theta_H) = R_{xx}/R_{xy}$ , directly reflects the ratio between the longitudinal scattering rate  $\tau^{-1}$  and the Hall scattering rate  $\tau_H^{-1}$ . In conventional Fermi liquids, these two rates typically follow the same temperature dependence. However, as shown in the inset of Figure 3a, a significant scattering rate separation in the optimally doped device ( $n_{2D} = 12.5 \times 10^{13} \text{ cm}^{-2}$ ) was observed. While  $R_{xx}$  exhibits a quasi-linear temperature dependence ( $R_{xx} \propto T^{1.2}$ ), the Hall angle cotangent,  $\cot(\Theta_H)$ , clearly follows a  $T^2$  scaling law over a wide temperature range (see ‘‘Supplementary Section 6’’ for more details), which indicates that the scattering processes dominating the longitudinal resistivity and the Hall effect possess distinct microscopic origins and energy dependencies.

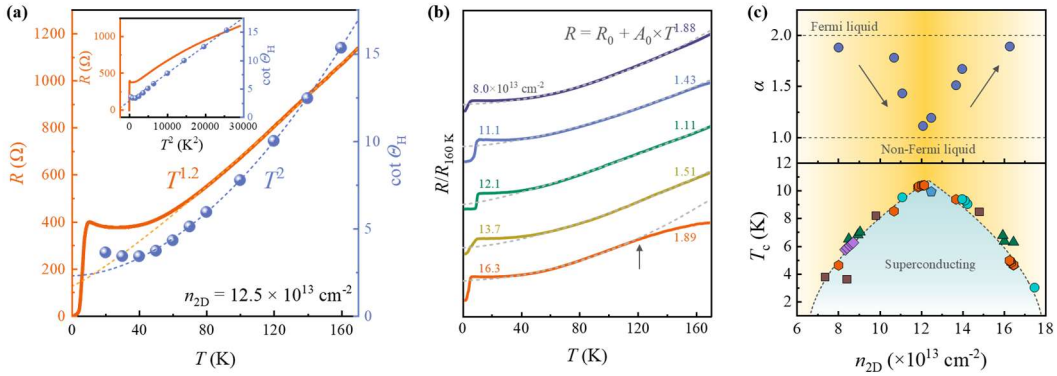


**Figure 4.** Non-Fermi liquid transport in superconducting MoS<sub>2</sub> devices. **(a)** Quasi-linear temperature dependence of resistance ( $R$ ) and  $T^2$ -dependent Hall angle cotangent  $\cot(\Theta_H)$  for an optimally doped device, demonstrating clear scattering-rate separation. Dashed lines are fits to  $R \propto T^{1.2}$  and  $\cot(\Theta_H) \propto T^2$ , respectively. Inset: The same data replotted against  $T^2$ , highlighting the quadratic scaling. **(b)**  $R$ - $T$  curves for superconducting MoS<sub>2</sub> at various carrier concentrations  $n_{2D}$ , spanning the underdoped to overdoped regimes. Dashed lines are fits to the power-law form  $R = R_0 + A \times T^\alpha$  in the indicated high-temperature regimes, demonstrating the systematic evolution of the

exponent  $\alpha$  with doping. (c) Doping dependence of the normal-state resistivity exponent  $\alpha$  (blue circles, upper) and the superconducting transition temperature  $T_c$  (lower). The “saddle-shaped” profile of  $\alpha$  mirrors the superconducting dome, indicating a strong correlation between non-Fermi liquid transport strength and superconductivity.

This separation of scattering rates between resistivity and Hall resistivity is one of the hallmark features of non-Fermi liquid (or strange metal) states in strongly correlated systems like cuprates<sup>[50, 51]</sup>, iron-based superconductors<sup>[6, 15]</sup>, and other systems<sup>[13, 26]</sup>, and is generally regarded as direct evidence for the breakdown of Fermi liquid theory due to quantum critical fluctuations. The observation of an identical behavior pattern in MoS<sub>2</sub> strongly suggests that the non-Fermi liquid transport of its normal state likewise stems from strong electron correlation effects, rather than conventional electron-phonon scattering.

To further examine the intrinsic connection between non-Fermi liquid transport and superconductivity in MoS<sub>2</sub>, we systematically studied the evolution of  $\alpha$  with  $n_{2D}$ . Figure 3b shows typical  $R$ - $T$  curves and their scaling analyses at different  $n_{2D}$  across the phase diagram. The results show that  $\alpha$  changes systematically with  $n_{2D}$ . In the underdoped region where superconductivity begins, the system largely follows the Fermi liquid picture ( $\alpha \sim 2$ ) across the whole temperature range. As  $n_{2D}$  increases into the optimal doping region,  $\alpha$  significantly deviates from 2, dropping into the range close to 1, manifesting as non-Fermi liquid transport, and shows significant deviation from the fit at lower temperatures ( $< 60$  K). Upon entering the overdoped region,  $\alpha$  gradually recovers to near 2, and returns to the Fermi liquid picture. Notably, an anomalous transition in resistance at high temperatures is observed at  $n_{2D} = 16.3 \times 10^{13} \text{ cm}^{-2}$ , possibly originating from charge density wave<sup>[29, 52-54]</sup> or bad metal behavior<sup>[26]</sup>, requiring further investigation.

Plotting both  $\alpha$  and superconducting critical temperature  $T_c$  as functions of  $n_{2D}$  in Figure 3c reveals that they evolve in a highly synchronized manner across the phase diagram. The index  $\alpha$  forms a “saddle-shaped” distribution in  $n_{2D}$  space, whose outline precisely coincides with the superconducting dome. The synchronous evolution of non-Fermi liquid transport and superconductivity in the MoS<sub>2</sub> phase diagram suggests they

may share a common physical origin. Meanwhile, the phenomenon that the strength of non-Fermi liquid transport in MoS<sub>2</sub> is positively correlated with the  $T_c$ , showing qualitative agreement with observations in strongly correlated superconductors like iron-based superconductors and cuprates<sup>[5, 14, 38, 40, 55]</sup>, indicating that electron-electron interactions play a key role in the superconducting mechanism of MoS<sub>2</sub>.

## Conclusion

In summary, this study achieves continuous doping control of superconducting MoS<sub>2</sub> from the underdoped to the overdoped regime using ionic liquid gating, and observes a symmetric superconducting dome whose critical exponents resemble those of strongly correlated superconductors. This similarity is further reflected in the  $T_c/T_F$  ratio of MoS<sub>2</sub>, which falls within the range characteristic of strongly correlated superconductors. Moreover, we uncover non-Fermi liquid behavior that co-evolves with superconductivity across the phase diagram, reaching its maximum strength where  $T_c$  peaks. This correspondence indicates a common physical origin for both phenomena. These findings establish ionic liquid-gated MoS<sub>2</sub> as an ideal platform with considerable electronic correlation and minimal competing orders, opening a new pathway to study the interplay between superconductivity and non-Fermi liquid transport.

## Method

**Device Fabrication and Characterization.** Thin MoS<sub>2</sub> flakes were mechanically exfoliated from bulk crystals (HQ Graphene) onto SiO<sub>2</sub> (285 nm)/Si substrates. Flakes of suitable thickness were identified via optical microscopy and confirmed by atomic force microscopy (Bruker Dimension Edge Inc.) and Raman spectroscopy.

The selected flakes were patterned into standard Hall bar geometries using a two-step electron beam lithography (EBL) process with a bilayer resist (Copolymer EL6/PMMA 495A8). The pattern was first defined by EBL (Crestec Inc.) and etched by reactive ion etching (Oxford Inc). Subsequent EBL, followed by electron-beam evaporation of Ti/Au (5/60 nm) contacts and liftoff in acetone, completed the device fabrication.

**Electrical Transport Measurements.** All electrical measurements were performed in a cryostat (TeslatronPT, Oxford Inc.). Electrical transport data were acquired using a Keithley 2634B source-measure unit for gate voltage and transfer curves, and a combination of a Keithley 6221 current source and a 2182A nanovoltmeter for other transport measurements. The use of a standard Hall bar geometry is critical for the accurate quantification of carrier concentration.

- [1] Keimer, B.; Kivelson, S. A.; Norman, M. R.; Uchida, S.; Zaanen, J. "From quantum matter to high-temperature superconductivity in copper oxides." *Nature* **2015**, *518*, 179.
- [2] Husain, A. A.; Mitrano, M.; Rak, M. S.; Rubeck, S.; Uchoa, B.; March, K.; Dwyer, C.; Schneeloch, J.; Zhong, R.; Gu, G. D.; et al. "Crossover of Charge Fluctuations across the Strange Metal Phase Diagram." *Phys. Rev. X* **2019**, *9*,
- [3] Greene, R. L.; Mandal, P. R.; Poniatowski, N. R.; Sarkar, T. "The Strange Metal State of the Electron-Doped Cuprates." *Annu. Rev. Condens. Matter Phys.* **2020**, *11*, 213.
- [4] Sachdev, S.; Chowdhury, D. "The novel metallic states of the cuprates: Topological Fermi liquids and strange metals." *Prog. Theor. Exp. Phys.* **2016**, *2016*, 12c102.
- [5] Yuan, J.; Chen, Q.; Jiang, K.; Feng, Z.; Lin, Z.; Yu, H.; He, G.; Zhang, J.; Jiang, X.; Zhang, X.; et al. "Scaling of the strange-metal scattering in unconventional superconductors." *Nature* **2022**, *602*, 431.
- [6] Huang, W. K.; Hosoi, S.; Čulo, M.; Kasahara, S.; Sato, Y.; Matsuura, K.; Mizukami, Y.; Berben, M.; Hussey, N. E.; Kontani, H.; et al. "Non-Fermi liquid transport in the vicinity of the nematic quantum critical point of superconducting FeSe<sub>1-x</sub>S<sub>x</sub>." *Phys. Rev. Res.* **2020**, *2*,
- [7] Kasahara, S.; Shibauchi, T.; Hashimoto, K.; Ikada, K.; Tonegawa, S.; Okazaki, R.; Shishido, H.; Ikeda, H.; Takeya, H.; Hirata, K.; et al. "Evolution from non-Fermi- to Fermi-liquid transport via isovalent doping in BaFe<sub>2</sub>(As<sub>1-x</sub>P<sub>x</sub>)<sub>2</sub> superconductors." *Phys. Rev. B* **2010**, *81*,
- [8] Chang, Y.-Y.; Paschen, S.; Chung, C.-H. "Mechanism of a strange metal state near a heavy-fermion quantum critical point." *Phys. Rev. B* **2018**, *97*,
- [9] Chang, Y. Y.; Hsu, F.; Kirchner, S.; Mou, C. Y.; Lee, T. K.; Chung, C. H. "Strange superconductivity near an antiferromagnetic heavy-fermion quantum critical point." *Phys. Rev. B* **2019**, *99*,
- [10] Taupin, M.; Paschen, S. "Are Heavy Fermion Strange Metals Planckian?" *Crystals* **2022**, *12*, 251.
- [11] Xia, Y.; Han, Z.; Zhu, J.; Zhang, Y.; Knüppel, P.; Watanabe, K.; Taniguchi, T.; Mak, K. F.; Shan, J. "Simulating high-temperature superconductivity in moiré WSe<sub>2</sub>." *arXiv* **2025**, *2508*,
- [12] Cao, Y.; Chowdhury, D.; Rodan-Legrain, D.; Rubies-Bigorda, O.; Watanabe, K.; Taniguchi, T.; Senthil, T.; Jarillo-Herrero, P. "Strange Metal in Magic-Angle Graphene with near Planckian Dissipation." *Phys. Rev. Lett.* **2020**, *124*,
- [13] Lyu, R.; Tuchfeld, Z.; Verma, N.; Tian, H.; Watanabe, K.; Taniguchi, T.; Lau, C. N.; Randeria, M.; Bockrath, M. "Strange metal behavior of the Hall angle in twisted bilayer graphene." *Phys. Rev. B* **2021**, *103*,
- [14] Zhang, R.; Qin, M.; Li, C.; Zhao, Z.; Wei, Z.; Xu, J.; Jiang, X.; Cheng, W.; Shi, Q.; Wang, X.; et al. "Correlation between unconventional superconductivity and strange metallicity revealed by operando superfluid density measurements." *Sci. Adv.* **2025**, *11*,
- [15] Čulo, M.; Berben, M.; Hsu, Y. T.; Ayres, J.; Hinlopen, R. D. H.; Kasahara, S.; Matsuda, Y.; Shibauchi, T.; Hussey, N. E. "Putative Hall response of the strange metal component in

- FeSe<sub>1-x</sub>S<sub>x</sub>." *Phys. Rev. Res.* **2021**, *3*,
- [16] Saito, Y.; Nakamura, Y.; Bahramy, M. S.; Kohama, Y.; Ye, J.; Kasahara, Y.; Nakagawa, Y.; Onga, M.; Tokunaga, M.; Nojima, T.; et al. "Superconductivity protected by spin–valley locking in ion-gated MoS<sub>2</sub>." *Nat. Phys.* **2015**, *12*, 144.
- [17] Lu, J. M.; Zheliuk, O.; Leermakers, I.; Yuan, N. F. Q.; Zeitler, U.; Law, K. T.; Ye, J. T. "Evidence for two-dimensional Ising superconductivity in gated MoS<sub>2</sub>." *Science* **2015**, *350*, 1353.
- [18] Xi, X.; Wang, Z.; Zhao, W.; Park, J.-H.; Law, K. T.; Berger, H.; Forró, L.; Shan, J.; Mak, K. F. "Ising pairing in superconducting NbSe<sub>2</sub> atomic layers." *Nat. Phys.* **2015**, *12*, 139.
- [19] Li, L. J.; O'Farrell, E. C. T.; Loh, K. P.; Eda, G.; Özyilmaz, B.; Castro Neto, A. H. "Controlling many-body states by the electric-field effect in a two-dimensional material." *Nature* **2015**, *529*, 185.
- [20] Xi, X.; Zhao, L.; Wang, Z.; Berger, H.; Forró, L.; Shan, J.; Mak, K. F. "Strongly enhanced charge-density-wave order in monolayer NbSe<sub>2</sub>." *Nat. Nanotechnol.* **2015**, *10*, 765.
- [21] Cho, K.; Kończykowski, M.; Teknowijoyo, S.; Tanatar, M. A.; Guss, J.; Gartin, P. B.; Wilde, J. M.; Kreyssig, A.; McQueeney, R. J.; Goldman, A. I.; et al. "Using controlled disorder to probe the interplay between charge order and superconductivity in NbSe<sub>2</sub>." *Nat. Commun.* **2018**, *9*,
- [22] Ye, J. T.; Zhang, Y. J.; Akashi, R.; Bahramy, M. S.; Arita, R.; Iwasa, Y. "Superconducting Dome in a Gate-Tuned Band Insulator." *Science* **2012**, *338*, 1193.
- [23] Piatti, E.; De Fazio, D.; Daghero, D.; Tamalampudi, S. R.; Yoon, D.; Ferrari, A. C.; Gonnelli, R. S. "Multi-Valley Superconductivity in Ion-Gated MoS<sub>2</sub> Layers." *Nano Lett.* **2018**, *18*, 4821.
- [24] Ding, D.; Qu, Z.; Han, X.; Han, C.; Zhuang, Q.; Yu, X.-L.; Niu, R.; Wang, Z.; Li, Z.; Gan, Z.; et al. "Multivalley Superconductivity in Monolayer Transition Metal Dichalcogenides." *Nano Lett.* **2022**, *22*, 7919.
- [25] Saito, Y.; Kasahara, Y.; Ye, J.; Iwasa, Y.; Nojima, T. "Metallic ground state in an ion-gated two-dimensional superconductor." *Science* **2015**, *350*,
- [26] Yang, Y.; Tao, Q.; Fang, Y.; Tang, G.; Yao, C.; Yan, X.; Jiang, C.; Xu, X.; Huang, F.; Ding, W.; et al. "Anomalous enhancement of the Nernst effect at the crossover between a Fermi liquid and a strange metal." *Nat. Phys.* **2023**, *19*, 379.
- [27] Yu, X.-L.; Wu, J. "Superconducting dome driven by intervalley phonon scattering in monolayer MoS<sub>2</sub>." *New J. Phys.* **2020**, *22*, 013015.
- [28] Das, T.; Dolui, K. "Superconducting dome in MoS<sub>2</sub> and TiSe<sub>2</sub> generated by quasiparticle-phonon coupling." *Phys. Rev. B* **2015**, *91*,
- [29] Giroto Erhardt, N.; Berges, J.; Poncé, S.; Novko, D. "Understanding the origin of superconducting dome in electron-doped MoS<sub>2</sub> monolayer." *npj 2D Mater. Appl.* **2025**, *9*,
- [30] Ghiotto, A.; Shih, E.-M.; Pereira, G. S. S. G.; Rhodes, D. A.; Kim, B.; Zang, J.; Millis, A. J.; Watanabe, K.; Taniguchi, T.; Hone, J. C.; et al. "Quantum criticality in twisted transition metal dichalcogenides." *Nature* **2021**, *597*, 345.
- [31] Chen, Q.; Lu, J.; Liang, L.; Zheliuk, O.; Ali El Yumin, A.; Ye, J. "Continuous Low-Bias Switching of Superconductivity in a MoS<sub>2</sub> Transistor." *Adv. Mater.* **2018**, *30*, 1800399.
- [32] Chen, Q.; Yan, C.; Lan, C.; Song, Q.; Yan, Y.; Wang, S. "Enhanced Backgate Tunability on Interfacial Carrier Concentration in Ionic Liquid-Gated MoS<sub>2</sub> Devices." *Small* **2025**,
- [33] Lu, J.; Zheliuk, O.; Chen, Q.; Leermakers, I.; Hussey, N. E.; Zeitler, U.; Ye, J. "Full superconducting dome of strong Ising protection in gated monolayer WS<sub>2</sub>." *Proc. Nat. Acad. Sci.* **2018**, *115*, 3551.
- [34] Zheliuk, O.; Lu, J. M.; Chen, Q. H.; Yumin, A. A. E.; Golightly, S.; Ye, J. T. "Josephson coupled Ising pairing induced in suspended MoS<sub>2</sub> bilayers by double-side ionic gating." *Nat. Nanotechnol.* **2019**, *14*, 1123.
- [35] Wan, W.; Harsh, R.; Dreher, P.; de Juan, F.; Ugeda, M. M. "Superconducting dome by tuning through a van

- Hove singularity in a two-dimensional metal." *npj 2D Mater. Appl.* **2023**, *7*,
- [36] Guo, Y.; Pack, J.; Swann, J.; Holtzman, L.; Cothrine, M.; Watanabe, K.; Taniguchi, T.; Mandrus, D. G.; Barmak, K.; Hone, J.; et al. "Superconductivity in 5.0° twisted bilayer WSe<sub>2</sub>." *Nature* **2025**, *637*, 839.
- [37] Xia, Y.; Han, Z.; Watanabe, K.; Taniguchi, T.; Shan, J.; Mak, K. F. "Superconductivity in twisted bilayer WSe<sub>2</sub>." *Nature* **2024**, *637*, 833.
- [38] Taillefer, L. "Scattering and Pairing in Cuprate Superconductors." *Annu. Rev. Condens. Matter Phys.* **2010**, *1*, 51.
- [39] Ando, Y.; Komiya, S.; Segawa, K.; Ono, S.; Kurita, Y. "Electronic Phase Diagram of High-*T<sub>c</sub>* Cuprate Superconductors from a Mapping of the In-Plane Resistivity Curvature." *Phys. Rev. Lett.* **2004**, *93*, 267001.
- [40] Božović, I.; He, X.; Wu, J.; Bollinger, A. T. "Dependence of the critical temperature in overdoped copper oxides on superfluid density." *Nature* **2016**, *536*, 309.
- [41] Nakagawa, Y.; Saito, Y.; Nojima, T.; Inumaru, K.; Yamanaka, S.; Kasahara, Y.; Iwasa, Y. "Gate-controlled low carrier density superconductors: Toward the two-dimensional BCS-BEC crossover." *Phys. Rev. B* **2018**, *98*,
- [42] Lin, X.; Zhu, Z.; Fauqué, B.; Behnia, K. "Fermi Surface of the Most Dilute Superconductor." *Phys. Rev. X* **2013**, *3*,
- [43] Kasahara, S.; Watashige, T.; Hanaguri, T.; Kohsaka, Y.; Yamashita, T.; Shimoyama, Y.; Mizukami, Y.; Endo, R.; Ikeda, H.; Aoyama, K.; et al. "Field-induced superconducting phase of FeSe in the BCS-BEC cross-over." *Proc. Nat. Acad. Sci.* **2014**, *111*, 16309.
- [44] Wang, Q.-Y.; Li, Z.; Zhang, W.-H.; Zhang, Z.-C.; Zhang, J.-S.; Li, W.; Ding, H.; Ou, Y.-B.; Deng, P.; Chang, K.; et al. "Interface-Induced High-Temperature Superconductivity in Single Unit-Cell FeSe Films on SrTiO<sub>3</sub>." *Chin. Phys. Lett.* **2012**, *29*, 037402.
- [45] Cao, Y.; Fatemi, V.; Fang, S.; Watanabe, K.; Taniguchi, T.; Kaxiras, E.; Jarillo-Herrero, P. "Unconventional superconductivity in magic-angle graphene superlattices." *Nature* **2018**, *556*, 43.
- [46] Rohr, F. O. v.; Orain, J.-C.; Khasanov, R.; Witteveen, C.; Nikitin, Z. S. A.; Chang, J.; Wieteska, A. R.; Pasupathy, A. N.; Amato, M. Z. H. A.; Luetkens, H.; et al. "Unconventional scaling of the superfluid density with the critical temperature in transition metal dichalcogenides." *Sci. Adv.* **2019**, *5*,
- [47] Uemura, Y. J. "Classifying superconductors in a plot of *T<sub>c</sub>* versus Fermi temperature *T<sub>F</sub>*." *Physica C* **1991**, *185*,
- [48] Uemura, Y. J. "Condensation, excitation, pairing, and superfluid density in high-*T<sub>c</sub>* superconductors: the magnetic resonance mode as a roton analogue and a possible spin-mediated pairing." *J. Phys.: Condens. Matter* **2004**, *16*, S4515.
- [49] Nakagawa, Y.; Kasahara, Y.; Nomoto, T.; Arita, R.; Nojima, T.; Iwasa, Y. "Gate-controlled BCS-BEC crossover in a two-dimensional superconductor." *Science* **2021**, *372*,
- [50] Chien, T.; Wang, Z.; Ong, N. "Effect of Zn impurities on the normal-state Hall angle in single-crystal YBa<sub>2</sub>Cu<sub>3-x</sub>Zn<sub>x</sub>O<sub>7-δ</sub>." *Phys. Rev. Lett.* **1991**, *67*, 2088.
- [51] Carrington, A.; Mackenzie, A. P.; Lin, C. T.; Cooper, J. R. "Temperature dependence of the Hall angle in single-crystal YBa<sub>2</sub>(Cu<sub>1-x</sub>Co<sub>x</sub>)<sub>3</sub>O<sub>7-δ</sub>." *Phys. Rev. Lett.* **1992**, *69*, 2855.
- [52] Rösner, M.; Haas, S.; Wehling, T. O. "Phase diagram of electron-doped dichalcogenides." *Phys. Rev. B* **2014**, *90*,
- [53] Bin Subhan, M. K.; Suleman, A.; Moore, G.; Phu, P.; Hoesch, M.; Kurebayashi, H.; Howard, C. A.; Schofield, S. R. "Charge Density Waves in Electron-Doped Molybdenum Disulfide." *Nano Lett.* **2021**, *21*, 5516.
- [54] Septianto, R. D.; Romagosa, A. P.; Dong, Y.; Matsuoka, H.; Ideue, T.; Majima, Y.; Iwasa, Y. "Gate-Controlled Potassium Intercalation and Superconductivity in Molybdenum Disulfide." *Nano Lett.* **2024**, *24*, 13790.
- [55] Jiang, X.; Qin, M.; Wei, X.; Xu, L.; Ke, J.; Zhu, H.; Zhang, R.; Zhao, Z.; Liang, Q.; Wei, Z.; et al. "Interplay between superconductivity and the strange-metal state in FeSe." *Nat. Phys.* **2023**, *19*, 365.

